Energy &
Environmental
Science

PAPER

View Article Online
View Journal | View Issue

Cite this: *Energy Environ. Sci.*, 2017, **10**, 2212

9.0% power conversion efficiency from ternary all-polymer solar cells†

Zhaojun Li,[a] Xiaofeng Xu,*[a] Wei Zhang,[b] Xiangyi Meng,[c] Zewdneh Genene,[d] Wei Ma,[c] Wendimagegn Mammo,[d] Arkady Yartsev,[b] Mats R. Andersson,[e] René A. J. Janssen*[f] and Ergang Wang*[a]

Received 4th July 2017,
Accepted 23rd August 2017

DOI: 10.1039/c7ee01858d

rsc.li/ees

Integration of a third component into a single-junction polymer solar cell (PSC) is regarded as an attractive strategy to enhance the performance of PSCs. Although binary all-polymer solar cells (all-PSCs) have recently emerged with compelling power conversion efficiencies (PCEs), the PCEs of ternary all-PSCs still lag behind those of the state-of-the-art binary all-PSCs, and the advantages of ternary systems are not fully exploited. In this work, we realize high-performance ternary all-PSCs with record-breaking PCEs of 9% and high fill factors (FF) of over 0.7 for both conventional and inverted devices. The improved photovoltaic performance benefits from the synergistic effects of extended absorption, more efficient charge generation, optimal polymer orientations and suppressed recombination losses compared to the binary all-PSCs, as evidenced by a set of experimental techniques. The results provide new insights for developing high-performance ternary all-PSCs by choosing appropriate donor and acceptor polymers to overcome limitations in absorption, by affording good miscibility, and by benefiting from charge and energy transfer mechanisms for efficient charge generation.

Broader context

All-polymer solar cells (all-PSCs), incorporating an active layer based on a blend of an electron-donor (D) polymer and an electron-acceptor (A) polymer, have drawn tremendous attention in the past few years. The use of polymer acceptors overcomes some disadvantages of the commonly used fullerene acceptors. However, the intrinsic narrow absorption widths of polymeric semiconductors make it challenging for single-junction all-PSCs to fully cover the solar irradiation spectrum. This is one of the key factors that constrain the photocurrent and power conversion efficiencies (PCEs) of all-PSCs. One facile solution is to employ donor and acceptor polymers with complementary absorption to construct a ternary all-PSC. However, there has been no successful example of ternary all-PSCs outperforming the state-of-the-art binary all-PSCs to date. In this work, we develop an appropriate combination of donor and acceptor polymers for high-performance ternary all-PSCs, which attain record-breaking PCEs of 9% for the first time.

Introduction

Polymer solar cells (PSCs) are capable of realizing large-area solar panels with low cost, light weight and good mechanical flexibility as well as relatively short energy payback time. As a result, they have drawn tremendous attention in the last few decades as one of the next-generation photovoltaic technologies.[1,2] A typical PSC contains a bulk-heterojunction (BHJ) active layer with a conjugated polymer as an electron–donor (D) and a fullerene derivative as an electron–acceptor (A).[3] Over the years, the power conversion efficiencies (PCEs) of single-junction PSCs have been steadily improved to >11%, particularly due to the development of high-performing donor polymers,[4] where the prevailing electron acceptors are still fullerene derivatives such as phenyl-C_{71}-butyric acid–methyl ester ($PC_{71}BM$).[5,6] Although $PC_{71}BM$ features high electron mobility and good

---

[a] Department of Chemistry and Chemical Engineering, Chalmers University of Technology, SE-412 96, Göteborg, Sweden. E-mail: xixu@chalmers.se, ergang@chalmers.se
[b] Division of Chemical Physics, Lund University, Box 124, SE-221 00 Lund, Sweden
[c] State Key Laboratory for Mechanical Behavior of Materials, Xi'an Jiaotong University, Xi'an 710049, China
[d] Department of Chemistry, Addis Ababa University, P. O. Box 33658, Addis Ababa, Ethiopia
[e] Flinders Centre for Nanoscale Science and Technology, Flinders University, Sturt Road, Bedford Park, Adelaide, SA 5042, Australia
[f] Molecular Materials and Nanosystems and Institute for Complex Molecular Systems, Eindhoven University of Technology, PO Box 513, 5600 MB Eindhoven, The Netherlands. E-mail: r.a.j.janssen@tue.nl

† Electronic supplementary information (ESI) available. See DOI: 10.1039/c7ee01858d

miscibility with most donor materials, it has intrinsic drawbacks such as high synthetic cost, weak absorption, undesired band gaps and morphological instability, which have still not been completely resolved.[7,8] Driven by the need to find alternative acceptors for $PC_{71}BM$, several material combinations have been developed to construct non-fullerene organic solar cells.[9–11] Among them, all-polymer solar cells (all-PSCs), incorporating donor and acceptor polymers in BHJ blends, have received considerable attention due to their unique properties such as low-cost production, readily tunable absorption and energy levels, good morphological stability as well as mechanical durability.[12–14] So far, growing efforts have been devoted to the synthesis of new acceptor polymers and to modulating blend morphology.[15–18] In the past five years, PCEs of all-PSCs have been rapidly improved from 2% to 9%.[19–22] However, the photocurrents of all-PSCs have been constrained mainly due to the intrinsic narrow absorption widths of polymeric semiconductors, which makes it challenging for single-junction all-PSCs to fully cover the solar irradiation spectrum.[13,23] To circumvent this constraint, one facile solution is to use a ternary approach by combining two donor polymers having complementary absorption spectra with an acceptor to construct a ternary solar cell.[24–28] So far, $PC_{71}BM$ and/or small molecule acceptors (SMAs) have been primarily used as acceptors for ternary systems,[29–37] which have shown great progress in photovoltaic performance and stability as compared to the corresponding binary PSCs.[38–50] However, the synthesis and purification of $PC_{71}BM$ and some SMAs with complicated structures are inherently time-consuming with high synthetic costs.[7,51] Polymer acceptors, on the other hand, are generally easy to synthesize and scale up with lower synthetic costs by using new techniques.[1,13,52] Moreover, polymer acceptors also afford better film-forming properties as well as robust mechanical and thermal stability of the active layers.[13,23]

Despite the inspiring advances in binary all-PSCs, there is no successful example of ternary all-PSCs outperforming the state-of-the-art binary all-PSCs. One of the key reasons is the suboptimal morphology generated in the multi-polymer blend films, since the intimate mixing of polymer chains is energetically unfavourable due to the interplay between the entropy and enthalpy of mixing.[53] In 2015, Jenekhe *et al.* developed a ternary system composed of the high-performing donor polymer PBDTTT-C-T and two selenophene-based acceptor polymers, resulting in a PCE of 3.2%.[54] Following this, a ternary all-PSC was constructed by combining a high band gap polymer PCDTBT with a low band gap PTB7-Th:N2200 blend, where PCDTBT served as a visible sensitizer and strongly contributed to the photocurrent and PCEs.[55,56] The resulting ternary all-PSCs attained a high short-circuit current density (J_{sc}) of 14.4 mA cm^{-2} and a decent PCE of 6.7%.[56] Using the same ternary approach, Li *et al.* recently realized a ternary all-PSC which achieved a maximum PCE of 7.2% with an outstanding J_{sc} of 15.7 mA cm^{-2}.[57] Although N2200 is the primarily used acceptor polymer in ternary all-PSCs, its poor morphological tenability tends to suppress the fill factors (FF) of the resulting all-PSCs.[20] So far, only a few binary all-PSCs have exhibited FF as high as 0.7,[19,20] and none of the ternary all-PSCs can register a decent FF of over 0.6, which discloses one of the key factors limiting the overall PCEs of ternary all-PSCs.[13,23]

In this work, we demonstrate high-performance ternary all-PSCs by incorporating high band gap poly[[4,8-bis[5-((2-octyl)-thio)thiophen-2-yl]benzo-[1,2-*b*:4,5-*b*′]dithiophene-2,6-diyl]]-*alt*-[bis(5-thiophen-2-yl)-5,6-difluoro-2-(2-hexyldecyl)-2*H*-benzo[*d*]-[1,2,3]triazole-4,7-diyl] (PBDTTS-FTAZ) as the second donor into poly[[4,8-bis[5-(2-ethylhexyl)-2-thienyl]benzo[1,2-*b*:4,5-*b*′]dithiophene-*alt*-(4-(2-ethylhexyl)-3-fluorothieno[3,4-*b*]thiophene)-2-carboxylate-2,6-diyl]] (PTB7-Th) and PNDI-T10 blends. Through optimizing the weight loadings of PBDTTS-FTAZ, the ternary all-PSCs attain a high J_{sc} of 14.4 mA cm^{-2}, an unprecedented FF of 0.74 and PCEs as high as 9.0% in both conventional and inverted devices. To our knowledge, this is among the best photovoltaic performances recorded for ternary all-PSCs to date.

Results and discussion

Polymer design and characterization

The structures of PTB7-Th, PBDTTS-FTAZ and PNDI-T10 are depicted in Fig. 1a. We recently designed a random acceptor polymer PNDI-T10, which featured reduced backbone rigidity and crystallinity, and thus improved solubility and molecular weight as compared to the widely used acceptor N2200 with an alternating backbone.[20] As a result, the PTB7-Th:PNDI-T10 all-PSCs delivered a high PCE of 7.6% with an extraordinarily high FF of 0.71, superior to the performance of PTB7-Th:N2200 all-PSCs.[20] We also developed a high band gap polymer PBDTTS-FTAZ with strong absorption in the wavelength region of 450–650 nm, which attained one of the highest PCEs among the $PC_{71}BM$-based PSCs incorporating donor polymers with band gaps >1.9 eV.[58] Since we notice that the absorption of the PTB7-Th:PNDI-T10 blend is very weak in the visible region, it is appropriate to use the ternary approach by introducing PBDTTS-FTAZ as the second donor into the PTB7-Th:PNDI-T10 blend to complement the absorption in the visible region. Thus, this ternary system is formed by using PTB7-Th as the primary donor (D_1), PBDTTS-FTAZ as the second donor (D_2), and PNDI-T10 as the acceptor (A). The ratio of PTB7-Th : PNDI-T10 is fixed to be 1 : 1, where the content of PBDTTS-FTAZ with respect to PTB7-Th is varied to optimize the $D_1 : D_2 : A$ ratios. The molecular weights and polydispersity indices of the polymers are listed in Table S1 in the ESI.†

Differential scanning calorimetry (DSC) was employed to investigate the thermal properties of the polymers and compatibility of the blends. As depicted in Fig. S1 in the ESI,† there is no detectable thermal transition for the neat PTB7-Th and PBDTTS-FTAZ films, whereas the neat PNDI-T10 film presents a melting transition temperature of 290 °C upon heating, and a crystallization temperature of 267 °C upon cooling.[20] There is no thermal transition observed in the 1 : 0.15 : 1 ternary blend, implying that large crystals in PNDI-T10 are suppressed and the miscibility of the donor and acceptor polymers should be reasonably good.

UV-vis-NIR absorption of the pristine polymers and ternary blends was measured to study the variations in absorption

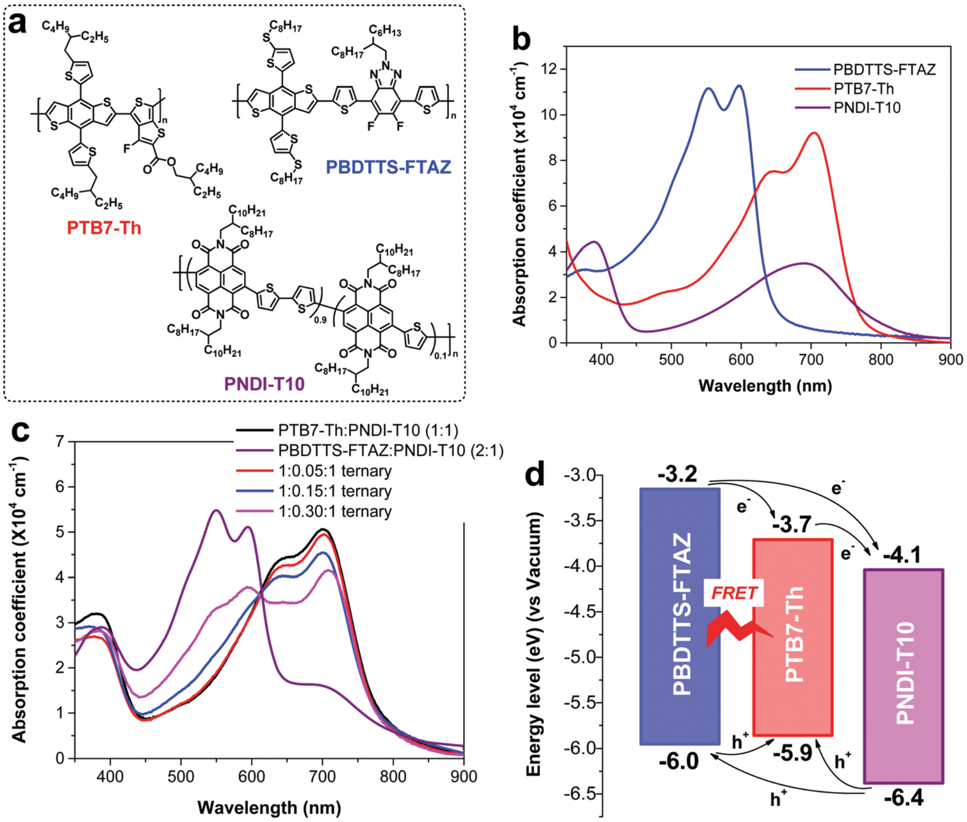

Fig. 1 (a) Polymer structures. (b) Absorption coefficients of the polymers in thin films. (c) Absorption coefficients of the binary and ternary blends. (d) Energy level diagram of the polymers.

as a function of different loadings of PBDTTS-FTAZ in the ternary blends. As depicted in Fig. 1b, the absorption spectra of PTB7-Th and PNDI-T10 are mostly overlapped in the wavelength region of 550–850 nm. In the thin film, the maximal absorption coefficient of PTB7-Th is around 9×10^4 cm^{-1} at 707 nm, much higher than that of PNDI-T10 at the same wavelength. PBDTTS-FTAZ, the second donor, presents strong absorption in the visible region of 450–650 nm with a higher absorption coefficient of 11×10^4 cm^{-1} at 600 nm, which is well complementary with the absorption of PTB7-Th and PNDI-T10. Fig. 1c illustrates that the absorption spectra of the ternary blends are gradually broadened when the content of PBDTTS-FTAZ is increased, which is in congruence with our expectation that inclusion of PBDTTS-FTAZ could improve the absorption of the ternary blends in the visible region.

To illustrate the charge/energy transfer pathways in the ternary system, the HOMO and LUMO levels of the three polymers were measured by using square wave voltammetry (SWV) (Fig. S2, ESI†).[59] As depicted in Fig. 1d, the LUMO levels of the three polymers provide a cascade alignment for electron transfer, while the HOMO levels do not align in a cascade fashion for hole transfer. The HOMO and LUMO levels of PTB7-Th fall in between those of PBDTTS-FTAZ. The slightly up-shifted HOMO level of PTB7-Th indicates that the majority of holes generated in PBDTTS-FTAZ may finally be transferred to the HOMO of PTB7-Th before extraction. The HOMO–HOMO and LUMO–LUMO energy offsets of each donor and acceptor pair are large enough (>0.3 eV) to guarantee sufficient driving force for efficient exciton dissociation.[60]

Photovoltaic device characterization

The ternary all-PSCs, with both conventional and inverted device structures, were investigated by using PBDTTS-FTAZ and PTB7-Th as donors and PNDI-T10 as the acceptor. The J–V characteristics of the all-PSCs under an illumination of AM 1.5G simulated solar light at 100 mW cm^{-2} are shown in Fig. 2a, c and Fig. S3a, c in the ESI.† As summarized in Fig. S4 and Table S4 in the ESI,† the device performance was optimized by varying the solvent annealing time of the active layers. The corresponding device parameters are summarized in Table 1 and Tables S2 and S3 in the ESI.† It is worth noting that, the PTB7-Th:PNDI-T10 binary all-PSCs exhibit PCEs of over 7% with an open-circuit voltage (V_{oc}) of around 0.8 V, a J_{sc} of around 12.8 mA cm^{-2} and a FF of around 0.7, which agree well with our previous report.[20] On the other hand, the PBDTTS-FTAZ:PNDI-T10 binary all-PSCs exhibit a higher V_{oc} of around 0.9 V due to the deeper HOMO level of PBDTTS-FTAZ, but lower J_{sc} and FF which lead to PCEs of 6–7%.[61] Fig. 2e illustrates the variations of the device parameters as a function of the content of PBDTTS-FTAZ, where both the conventional and inverted devices present the same trend. The J_{sc}, FF and PCEs are gradually improved as the content of PBDTTS-FTAZ is increased from 0 to 15%. Then, these

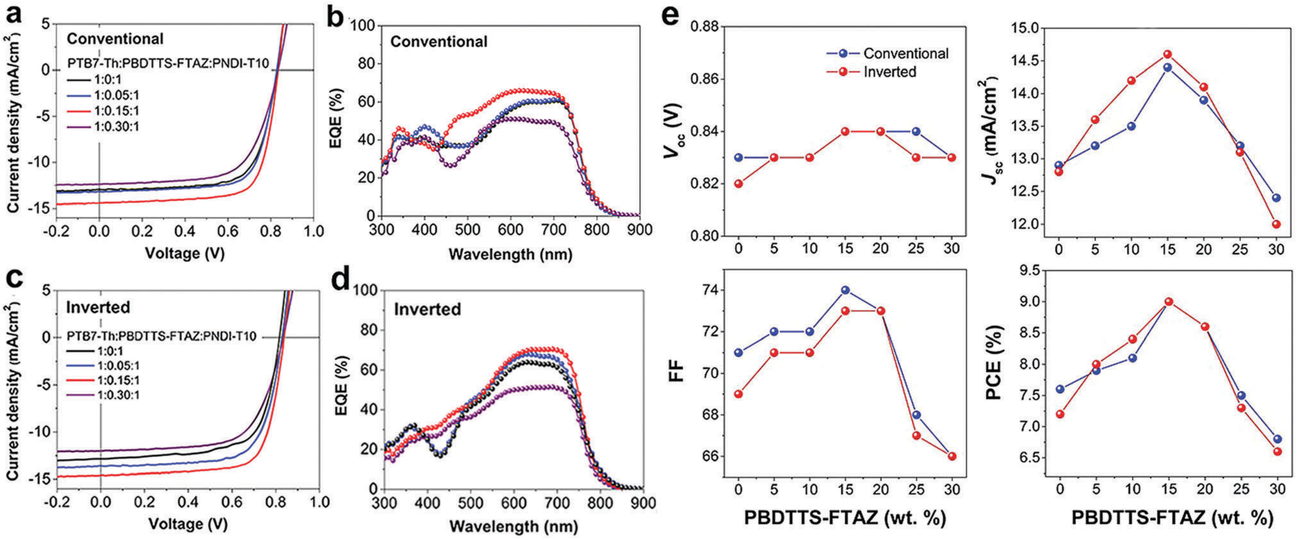

Fig. 2 (a and b) J–V characteristics and corresponding EQE spectra of conventional all-PSCs; (c and d) J–V characteristics and corresponding EQE spectra of inverted all-PSCs; (e) variations in V_{oc}, J_{sc}, FF and PCEs of the binary and ternary all-PSCs as a function of the content of PBDTTS-FTAZ.

Table 1 Photovoltaic parameters of the conventional and inverted all-PSCs

	Conventional[a]				Inverted[b]			
$D_1:D_2:A$[c]	V_{oc} (V)	J_{sc} (mA cm^{-2})	FF	PCE (%)	V_{oc} (V)	J_{sc} (mA cm^{-2})	FF	PCE (%)
1 : 0 : 1	0.83	12.9 (12.5)[d]	0.71	7.6[e] (7.4)[f]	0.82	12.8 (12.5)[d]	0.69	7.2[e] (7.0)[f]
1 : 0.05 : 1	0.83	13.2 (13.0)	0.72	7.9 (7.5)	0.83	13.6 (13.3)	0.71	8.0 (7.6)
1 : 0.10 : 1	0.83	13.5 (13.4)	0.72	8.1 (7.8)	0.83	14.2 (13.6)	0.71	8.4 (8.0)
1 : 0.15 : 1	0.84	14.4 (14.5)	0.74	9.0 (8.6)	0.84	14.6 (14.1)	0.73	9.0 (8.5)
1 : 0.20 : 1	0.84	13.9 (14.2)	0.73	8.6 (8.2)	0.84	14.1 (13.4)	0.73	8.6 (8.1)
1 : 0.25 : 1	0.84	13.2 (12.8)	0.68	7.5 (7.2)	0.83	13.1 (12.9)	0.67	7.3 (6.9)
1 : 0.30 : 1	0.83	12.4 (12.1)	0.66	6.8 (6.2)	0.83	12.0 (10.8)	0.66	6.6 (6.2)
0 : 2 : 1	0.90	11.6 (12.2)	0.57	6.0 (5.8)	0.89	12.3 (12.2)	0.63	6.9 (6.6)

[a] Device structure: ITO/PEDOT:PSS (40 nm)/active layer/LiF (1 nm)/Al (100 nm). [b] Device structure: ITO/ZnO (40 nm)/active layer/MoO_3 (10 nm)/Ag (100 nm). [c] D_1 is PTB7-Th; D_2 is PBDTTS-FTAZ; A is PNDI-T10. [d] Photocurrent calculated by integrating the EQE spectra with the AM 1.5G solar spectrum. [e] Maximal PCE. [f] Average PCE of ten devices.

parameters dramatically decrease when the PBDTTS-FTAZ content is further increased from 15% to 30%. Thus, the 1 : 0.15 : 1 ternary all-PSCs attain the maximal PCEs of 9.0%, with an unvaried V_{oc} of 0.84 V, a clearly enhanced J_{sc} of 14.5 mA cm^{-2}, and a slightly improved FF of 0.74. The PCEs are improved by 18% as compared to the PTB7-Th:PNDI-T10 binary all-PSCs (9.0% *vs.* 7.6%), which are mainly due to the 10% increase in J_{sc}. The nearly constant V_{oc} is pinned to that of the PTB7-Th:PNDT-T10 solar cells rather than staying between the two extremes. We attribute this to the mechanism that the majority of holes are transferred to the HOMO of PTB7-Th before extraction. Holes may rarely have the chance to be extracted from the HOMO of PBDTTS-FTAZ to the anode, otherwise a dependence of V_{oc} on the loading of PBDTTS-FTAZ should be observed. Similar phenomena were observed in several ternary systems featuring comparable energy level alignments to this work.[26,41,56] So far, the device stability of all-PSCs has not been widely investigated.[15,18,61] A preliminary stability study is conducted in this work. As shown in Fig. S5, S6 and Tables S5, S6 in the ESI,† undesired fast decay in PCEs is observed when the devices are stored at 20 °C or undergo thermal annealing at 80 °C in a glovebox.

According to our previous report, the PTB7-Th:PNDI-T10 blends presented clearly higher hole and electron mobilities than those of the PBDTTS-FTAZ:PNDI-T10 blends.[20,61] Inclusion of 5–30% of PBDTTS-FTAZ in the ternary blends still retains similar charge mobilities to those of the PTB7-Th:PNDI-T10 binary blends (Fig. S7 and Table S7, ESI†). The hole and electron mobilities on the order of 10^{-4} cm^2 V^{-1} s^{-1} are relatively high and well balanced in this ternary system, indicating that mobility is not a limiting factor for the photovoltaic performance.[62] This partially explains the comparatively high FF (>0.7) in both the PTB7-Th:PNDI-T10 binary and the ternary all-PSCs.

It would be interesting to verify the actual composition in the ternary blend by using the facile method developed in our previous work.[61] The actual compositions in the ternary blend can be calculated by using the simulated absorption of the individual polymers in the blend films (Fig. S8 and Table S8, ESI†) and the measured absorption coefficients of the neat polymer films (Fig. 1b). Thus, the actual compositions of the

1 : 0.05 : 1, 1 : 0.15 : 1 and 1 : 0.3 : 1 ternary blends are calculated to be 1 : 0.03 : 0.96, 1 : 0.16 : 0.99 and 1 : 0.27 : 1.03 by volume, respectively. Assuming that the three polymers have the same density and ignoring the influences of chain orientations on absorption coefficients, the actual compositions are in good agreement with the feed ratios of the polymer solutions for spin-coating.

To study the spectral response of the all-PSCs and the accuracy of the measured J_{sc}, external quantum efficiency (EQE) spectra of the binary and ternary all-PSCs were measured (Fig. 2b, d and Fig. S3b, d, ESI†). Compared to the PTB7-Th:PNDI-T10 binary all-PSCs, the EQE response of the 1 : 0.15 : 1 ternary all-PSCs shows substantial improvement in the wavelength region of 450–800 nm, where the maximal EQEs surpass 65% in both the conventional and inverted devices. The enhanced EQE profiles in the wavelength region of 450–650 nm, where PBDTTS-FTAZ features the prominent absorption, indicate that the increase in J_{sc} for the 1 : 0.15 : 1 ternary all-PSCs can be ascribed to the enhanced light absorption of PBDTTS-FTAZ. Since PBDTTS-FTAZ can only improve the absorption in the visible region, the increased EQEs in the longer wavelength of 650–800 nm imply that either the photon conversion efficiency of the PTB7-Th:PNDI-T10 junction is slightly enhanced, or more free charges are generated and collected due to the charge and/or energy transfer from PBDTTS-FTAZ to PTB7-Th. On the other hand, the 1 : 0.05 : 1 and 1 : 0.30 : 1 ternary all-PSCs show lower EQE profiles compared with the 1 : 0.15 : 1 ternary all-PSCs probably due to the suboptimal morphology. For all the devices, the J_{sc} values calculated by integrating the EQE spectra with the AM 1.5G solar spectrum are in good agreement with the measured J_{sc} values from the J–V curves, exhibiting small mismatches of less than 5%. Compared with the PTB7-Th:PNDI-T10 binary all-PSCs, the clearly higher J_{sc} calculated from EQE attests to the fact that the inclusion of PBDTTS-FTAZ can boost the J_{sc} in this ternary system. To clarify the effects of PBDTTS-FTAZ on this ternary system, we choose to investigate three PBDTTS-FTAZ loadings (5%, 15% and 30%) as described below.

Photophysical characterization

To study the exciton dissociation process in the ternary system, we conducted steady-state photoluminescence (PL), time-resolved photoluminescence (TRPL) and absolute fluorescence quantum yield measurements. As depicted in Fig. 3a, the PBDTTS-FTAZ:PNDI-T10 and PTB7-Th:PNDI-T10 binary blends show tiny PL peaks at 725 nm and 830 nm, respectively, whereas the PL of each polymer is completely quenched in the 1 : 0.15 : 1 ternary blend. This suggests that the inclusion of PBDTTS-FTAZ promotes exciton dissociation in the ternary blend as compared to the binary blends. Since PBDTTS-FTAZ and PTB7-Th present distinct PL spectra, the TRPL decay of the 1 : 0.15 : 1 ternary blend was probed at two wavelengths to study the different exciton dissociation dynamics induced by the two donor polymers (Fig. 3b). When the ternary blend is probed at 690 nm, where PBDTTS-FTAZ has the predominant emission, the TRPL kinetics shows a single-exponential behavior with a very fast decay within 3 ps. When it is probed at 805 nm, where the emission is dominated by PTB7-Th and PNDI-T10, a much

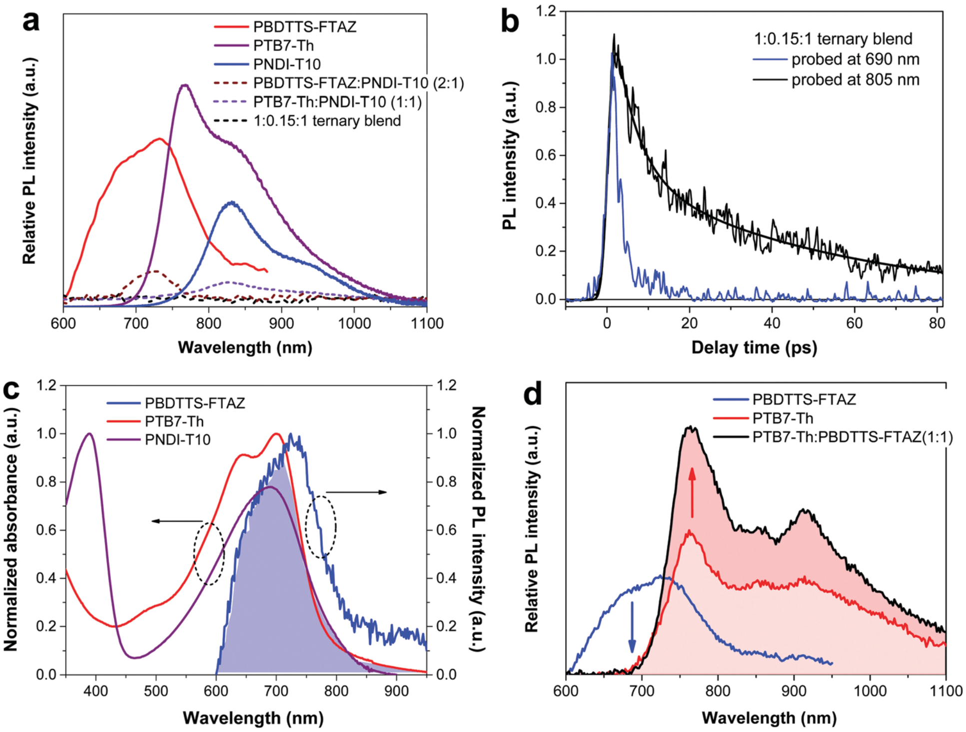

Fig. 3 (a) Steady-state PL spectra of the neat polymers and ternary films excited at 500 nm. (b) Kinetic traces of PL from the ternary 1 : 0.15 : 1 film excited at 400 nm. (c) Absorption spectra of neat PTB7-Th, neat PNDI-T10 film and PL spectrum of neat PBDTTS-FTAZ film. (d) PL spectra of neat PBDTTS-FTAZ, neat PTB7-Th film and PBDTTS-FTAZ:PNDI-T10 blend film.

slower PL decay with a lifetime of over 20 ps is observed, which combines a bi-exponential behavior with a fast and a slow component.[18,20,61] The TRPL results reveal that, in the 1 : 0.15 : 1 ternary blend, the generated excitons in PBDTTS-FTAZ can be efficiently dissociated *via* charge and/or energy transfer, whereas the generated excitons in PTB7-Th and PNDI-T10 may not be equally dissociated with the same efficiency.[18,61]

To study the energy transfer mechanism in this ternary system, Fig. 3c depicts that the absorption spectra of PTB7-Th and PNDI-T10 overlap well with the PL spectrum of PBDTTS-FTAZ. This is a spectral indication of Förster resonant energy transfer (FRET) from PBDTTS-FTAZ to PTB7-Th and PNDI-T10. Since FRET is a non-radiative energy transfer through a long-range dipole–dipole coupling, it requires spectral overlap between the emission of the energy donor and the absorption of the energy acceptor. In order to gain insights into the FRET between the two donor polymers, the PBDTTS-FTAZ:PTB7-Th blend was excited at two wavelengths. When excited at 500 nm, the PBDTTS-FTAZ:PTB7-Th blend shows a clearly higher PL intensity compared to the neat PTB7-Th film, while the PL of PBDTTS-FTAZ completely disappears in the blend (Fig. 3d). In contrast, when excited at 700 nm, very similar PL spectra are observed in the neat PTB7-Th and PBDTTS-FTAZ:PTB7-Th blend films (Fig. S9, ESI†). This distinct PL response at different excitation wavelengths reveals that energy transfer from PBDTTS-FTAZ to PTB7-Th occurs, but not the other way round. We should point out that there is a competition between the energy transfer from PBDTTS-FTAZ to PTB7-Th and the charge transfer from PBDTTS-FTAZ to PNDI-T10 in the ternary blends. As reported in many ternary systems, the energy and charge transfer processes are often intertwined.[26]

Associated with the energy level diagram, device performance and photophysical study, we can gain a clear insight into the energy and charge transfer pathways in this ternary system. The energy transfer from PBDTTS-FTAZ to PTB7-Th contributes extra excitons to PTB7-Th, which can be efficiently dissociated at the interface of PTB7-Th:PNDI-T10. For the charge transfer, all the holes are energetically favoured to be transferred to PTB7-Th due to its highest HOMO level, which well explains that the measured V_{oc} values of the ternary all-PSCs are pinned to that of the PTB7-Th:PNDI-T10 all-PSCs.[26,41,63] Because of the desired LUMO levels and sufficient LUMO–LUMO offset in this ternary system, electrons can be efficiently generated at the interface of each donor and PNDI-T10, and then transferred and collected at the cathode.

Morphology study

It is known that device performance is highly dependent on the morphology of the active layers. Therefore, a detailed analysis of the nanostructure variations induced by the second donor in the ternary blends was performed using atomic force microscopy (AFM) and grazing incidence wide angle X-ray scattering (GIWAXS). All the blend films were prepared under optimized device conditions. The AFM images reveal that the 1 : 0.05 : 1 and 1 : 0.15 : 1 ternary blend films form smooth surfaces with small root-mean-square (RMS) roughness values of 1.0 nm and 1.6 nm, respectively, which are similar to the RMS of the PTB7-Th:PNDT-T10 binary blend.[20] On the other hand, inclusion of 30% PBDTTS-FTAZ causes the RMS roughness to increase to 2.5 nm (Fig. S10, ESI†). The morphological stability of the 1 : 0.15 : 1 ternary blend was studied by varying the solvent annealing time, thermal annealing time and storage time, to have a better understanding of the stability of device performance. As depicted in the AFM images in Fig. S11 in the ESI,† visible morphology changes can be found when solvent annealing was performed with different times, which correlates with the varied device performance as summarized in Fig. S4 and Table S4 in the ESI.† On the other hand, there is no clear change observed for the 1 : 0.15 : 1 ternary blends along the thermal annealing time and storage time as shown in Fig. S12 and S13 in the ESI.† Fig. 4 depicts the 2D GIWAXS images and the line-cuts of GIWAXS patterns of the binary and ternary blend films. According to previous reports, the three neat polymer films (PTB7-Th, PBDTTS-FTAZ and PNDI-T10) showed

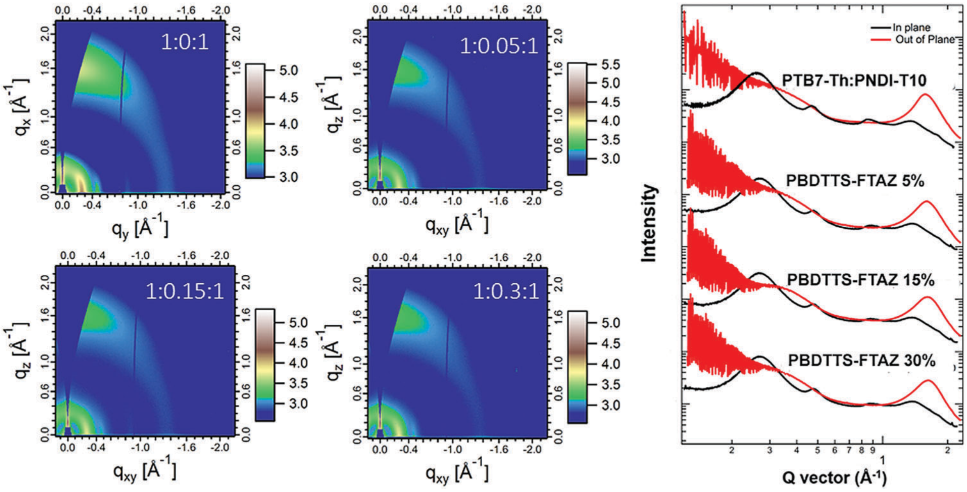

Fig. 4 GIWAXS 2D patterns and scattering profiles of the binary and ternary blend films.

a distinct (100) lamellae distance of around 2.3 nm with (100) peaks located at $q_{xy} \approx 0.26–0.27$ Å^{-1}. Along the out-of-plane direction, the neat PTB7-Th and PNDI-T10 films showed a similar π–π stacking distance of 0.39 nm with (010) peaks at $q_z \approx 1.60$ Å^{-1}. A slightly shorter π–π stacking distance of 0.36 nm was found in the neat PBDTTS-FTAZ film, with (010) peaks at $q_z \approx 1.75$ Å^{-1}.[20,58,64] As summarized in Tables S9 and S10 in the ESI,† each of the ternary blend films shows one broad (100) peak at $q_{xy} \approx 0.27$ Å^{-1} along the in-plane direction and one broad (010) peak at $q_z \approx 1.60$ Å^{-1} along the out-of-plane direction. This suggests that all the blend films have preferred face-on orientations with respect to the substrate. According to the line-cuts along the in-plane direction, the corresponding (100) *d*-spacing and (100) coherence lengths (CL) of the individual PTB7-Th and PNDI-T10 polymers have very little variations in the ternary blends, as the content of PBDTTS-FTAZ increases. Since the (010) peaks of the three polymers tend to fully overlap in all the ternary blends, it is difficult to distinguish the individual contribution of each polymer to the crystals. In this case, the domains in the blends should contain a mixture of crystallites from the three polymers. A similar (010) *d*-spacing of around 0.39 nm is observed in each of the blends, whereas the (010) CL values decreased slightly from 1.84 nm to 1.45 nm as the content of PBDTTS-FTAZ increases from 0 to 30%. The GIWAXS results reveal that the ternary blends present good miscibility and mostly retain the polymer orientations in the PTB7-Th:PNDI-T10 blend. As the content of PBDTTS-FTAZ increases, a slight decrease in crystallinity along the (010) direction is inevitable. Several reports revealed that the third component can act as a disordered phase and decrease the crystallinity of the polymers in the ternary blend as compared to the binary blend.[37,45] This increased disorder of polymer packing is also evidenced by the gradually reduced absorption coefficients of the ternary blends when the content of PBDTTS-FTAZ is increased. As the loading of PBDTTS-FTAZ is increased from 0 to 15%, increases in J_{sc} and PCEs are observed which can mainly be attributed to the enhanced light absorption from PBDTTS-FTAZ. As the loading of PBDTTS-FTAZ increases from 15% to 30%, it strengthens the interference on the π–π stacking of the PTB7-Th:PNDI-T10 blend, which seems to counteract the positive effects from the enhanced absorption. As we discuss in the recombination section below, when the content of PBDTTS-FTAZ exceeds 15%, it serves as a recombination centre in the ternary blend, which leads to a gradual decrease of the overall J_{sc}, FF and PCEs in the ternary all-PSCs.

Internal quantum efficiency and recombination

To evaluate the fraction of collected charge carriers per incident absorbed photon, the internal quantum efficiency (IQE) was calculated from the measured EQE of the all-PSCs, and the simulated absorptance spectra of the active layers. As shown in Fig. 5a, both the absorptance and IQE profiles of the 1 : 0.15 : 1 ternary all-PSC are clearly higher than those of the PTB7-Th:PNDI-T10 binary all-PSC throughout the whole absorption wavelength of 450–750 nm, which should stem from the synergistic effects of extra free charges contributed by PBDTTS-FTAZ, and the reduced charge recombination in the 1 : 0.15 : 1 ternary all-PSC. Associated with the EQE response, it can be claimed that the inclusion of small amounts of PBDTTS-FTAZ indeed leads to the enhanced J_{sc} in this ternary system. As discussed below, the saturated photocurrent *vs.* theoretical maximum photocurrent reveals that around 89% of the absorbed photons can be converted into free charges in the 1 : 0.15 : 1 ternary all-PSCs, which agrees well with the average IQE of ≈85% in the 1 : 0.15 : 1 ternary all-PSC.

To estimate the recombination losses, we calculated the theoretical maximum photocurrent density (J_{max}) of the conventional binary and ternary all-PSCs by integrating the simulated absorption of the active layers with the AM 1.5G solar spectrum, by assuming that all the absorbed photons by the active layer can be converted to a photocurrent (IQE = 100%). With the optimised active layer thickness of around 95 nm, the conventional PTB7-Th:PNDI-T10 all-PSC shows a J_{max} of 16.5 mA cm^{-2}, while a higher J_{max} of 17.0 mA cm^{-2} is recorded from the conventional 1 : 0.15 : 1 ternary all-PSC, clearly suggesting the contribution of the second donor to the enhanced photocurrent of the ternary all-PSC. Furthermore, the saturated photocurrent density (J_{sat}) of the all-PSCs was measured at high bias voltage (Fig. S14, ESI†). In principle, the inverted bias voltage can sweep out all the free charges in the active layers to the electrodes. When it approaches −1.5 V, the *J*–*V* curves of the 1 : 0.15 : 1 ternary all-PSCs show slow saturation with a higher

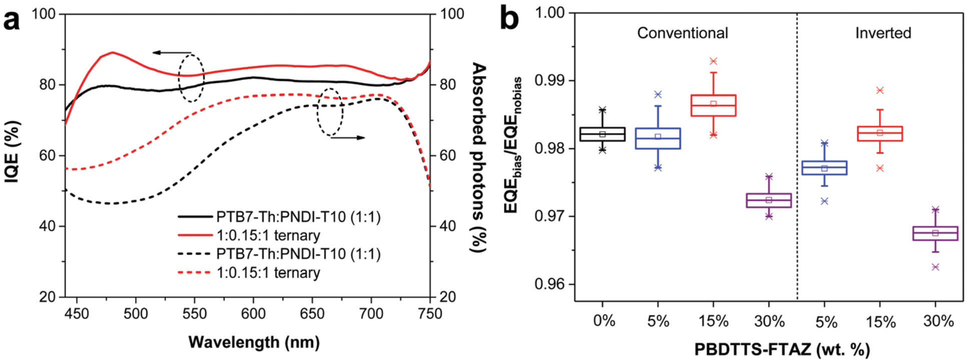

Fig. 5 (a) IQE curves of the PTB7-Th:PNDI-T10 binary and ternary all-PSCs. (b) Average EQE$_{bias}$/EQE$_{nobias}$ values of the all-PSCs with and without bias light.

J_{sat} of 15.1 mA cm^{-2}, as compared to 13.5 mA cm^{-2} for the conventional PTB7-Th:PNDI-T10 binary all-PSC. The geminate recombination loss (η_G) in the conventional 1 : 0.15 : 1 all-PSC is calculated to be $\approx$12%, which is inferred from the equation $\eta_G = 1 - (J_{sat}/J_{max})$,[61] by using a J_{sat} of 15.1 mA cm^{-2} and a J_{max} of 17.0 mA cm^{-2}. In contrast, the PTB7-Th:PNDI-T10 binary all-PSC features a higher η_G of $\approx$19%, by using a J_{sat} of 13.5 mA cm^{-2} and a J_{max} of 16.5 mA cm^{-2}.[20] This reveals that the optimized ternary all-PSC can suppress the geminate recombination.

To quantify the bimolecular recombination, EQEs were measured with or without the illumination of bias light for both the conventional and inverted devices (Fig. S15, ESI†). Since bimolecular recombination is strongly correlated with the charge carrier density, additional illumination can increase the charge carrier density in the film and stimulate bimolecular recombination under short-circuit conditions. Due to the agitated bimolecular recombination under the bias light, the corresponding EQE profile decreases as compared to the EQE without the bias light. The average ratio of the measured EQEs with and without the bias light (EQE_{bias}/EQE_{nobias}) in the whole EQE wavelength can quantitatively evaluate the bimolecular recombination of solar cells.[65] Fig. 5b illustrates the average values of EQE_{bias}/EQE_{nobias} in the conventional and inverted ternary all-PSCs. The average bimolecular recombination efficiency (η_{BR}) is denoted by $\eta_{BR} = EQE_{nobias}/EQE_{bias} - 1$.[20] The 1 : 0.15 : 1 ternary all-PSCs show the lowest η_{BR} of only 1–2% for both the conventional and inverted devices, implying that the bimolecular recombination in these all-PSCs is negligible. Impressively, the conventional 1 : 0.15 : 1 ternary all-PSC shows an even lower η_{BR} as compared with the reported η_{BR} in the conventional PTB7-Th:PNDI-T10 all-PSC.[20] Slightly higher η_{BR} is observed in the 1 : 0.05 : 1 and 1 : 0.30 : 1 ternary all-PSCs, which indicates that bimolecular recombination is aggravated in these two ternary all-PCSs. A comparison of the efficiencies of the geminate recombination ($\eta_G \approx 12\%$) and the bimolecular recombination ($\eta_{BR} \approx 2\%$) in the conventional 1 : 0.15 : 1 ternary all-PSC reveals that geminate recombination is still the primary loss under the short-circuit condition, but we should point out that the bimolecular recombination would gradually accumulate in the maximum power point of solar cells.[66] For the conventional 1 : 0.15 : 1 ternary all-PSC, the sum of η_G and η_{BR} ($\approx$14%) agrees well with the total recombination loss of $\approx$15%, which can be inferred from eqn (1) – (J_{sc}/J_{max}),[61] by using J_{sc} = 14.4 mA cm^{-2} and J_{max} = 17.0 mA cm^{-2}. On the other hand, a much larger total recombination loss of $\approx$22% (J_{sc} = 12.9 mA cm^{-2} and J_{max} = 16.5 mA cm^{-2}) is obtained from the conventional PTB7-Th:PNDI-T10 binary all-PSC.[20] The recombination study reveals that the optimized ternary all-PSC can reduce the geminate and bimolecular recombination as compared to the PTB7-Th:PNDI-T10 binary all-PSC, which spontaneously suppresses the overall recombination losses.

Conclusion

We have demonstrated that the photovoltaic performance of the PTB7-Th:PNDI-T10 all-PSC is improved by incorporating a high band gap polymer PBDTTS-FTAZ as the second donor. The optimized 1 : 0.15 : 1 ternary all-PSCs attain outstanding PCEs of 9.0% in both the conventional and inverted devices, achieving one of the highest PCEs for ternary all-PSCs and exhibiting 18% improvement as compared to the binary all-PSCs. PBDTTS-FTAZ, serving as a sensitizer in the visible region, broadens the absorption and generates more free charges by simultaneous charge and energy transfer. The optimized ternary blend presents extended absorption, optimal morphology and reduced recombination losses, all of which synergistically lead to the enhanced J_{sc}, unprecedented FF of 0.74 and high PCEs. Our work laid credence to the ternary approach as a facile and robust strategy to improve the performance of all-PSCs. It also highlights that PNDI-T10 is a promising acceptor polymer with good applicability in both binary and ternary all-PSCs.

Experimental section

PSC fabrication and characterization

Conventional all-PSCs were fabricated using the configuration of indium tin oxide (ITO)/PEDOT:PSS/active layer/LiF/Al. As a buffer layer, PEDOT:PSS (Baytron P VP Al 4083) was spin-coated onto ITO at a spin-coating rate of 3000 rpm for 60 s, followed by annealing at 150 °C for 10 minutes. The thickness of the PEDOT:PSS layer was around 40 nm, as determined using a Dektak 6 M surface profilometer. Different weight ratios of the donor and acceptor polymers were dissolved in chlorobenzene (CB) at 70 °C overnight. The active layer was spin-coated from the warm CB solution onto the PEDOT:PSS layer in a glove box. The total concentration of PTB7-Th, PBDTTS-FTAZ and PNDI-T10 was fixed as 11 mg mL^{-1}. After spin-coating, the films were transferred to a vapor deposition system inside a glove box. LiF (1 nm) and Al (100 nm) were sequentially deposited onto the active layers *via* a mask under 3×10^{-4} Pa vacuum. Inverted all-PSCs were fabricated using an indium tin oxide (ITO)/ZnO (40 nm)/Active layer/MoO_3 (10 nm)/Ag (100 nm) structure. Sol–gel ZnO was prepared by mixing zinc acetate dehydrate (0.5 M) and ethanolamine (0.5 M) in 2-methoxy ethanol for 1 h at room temperature. Sol–gel ZnO (thickness of around 40 nm, determined using a Dektak 6 M surface profilometer) was spin-coated onto an ITO-coated glass substrate at a spinning rate of 4000 rpm for 60 s, followed by annealing at 150 °C for 5 minutes. The active layer was then spin-coated on top of the ZnO layer in a glove box. After spin-coating, the films were transferred to a vapor deposition system inside a glove box. MoO_3 (10 nm) and Ag (100 nm) were deposited *via* a mask under 3×10^{-4} Pa vacuum onto the active layer. The active area of the device was 9 mm^2 or 16 mm^2, which was defined by the overlap of the ITO and Al electrode and was measured carefully using a microscope. For all the conventional and inverted ternary all-PSCs, the active layers were solvent annealed under a CB atmosphere for 1.5 h.

All the devices were tested in the glove box at 20 °C. The *J–V* curves were recorded in the backward scan direction and the efficiency was calculated from the *J–V* characteristics recorded using a Keithley 2400 source meter under illumination from a tungsten-halogen lamp filtered using a Hoya LB120 daylight filter at an intensity of 100 mW cm^{-2}, which was checked with a calibrated Si photodiode. Accurate J_{sc} values were determined under AM 1.5G conditions by integrating the EQE with the AM 1.5G solar spectrum.

EQE measurements were performed in a home-built setup. All devices were kept in a nitrogen-filled box with a quartz window, and illuminated through a circular aperture with 2 mm diameter. The white light of a 50 W tungsten halogen lamp (Osram 64610) was modulated with a mechanical chopper (Stanford Research, SR 540) and passed through a monochromator (Oriel, Cornerstone 130). For the EQE under bias light, a 530 nm high power LED (Thorlabs) was used to illuminate the solar cell simultaneously under the mechanically modulated monochromatic light and the unmodulated LED light. For both unbiased and biased EQE measurements, the differential photocurrent density was picked up by a lock-in amplifier. The current was recorded as the voltage over a 50 Ω resistance, and was converted to the EQE profile by comparing the data with a calibrated silicon reference cell.

Author contributions

Polymer synthesis and characterization were carried out by X. X. and Z. G. Device fabrication and evaluation were carried out by Z. L. TRPL and exciton quenching measurements were performed by W. Z. and A. Y. GIWAXS measurements were performed by X. M. and W. M. R. J., M. A. and W. M. involved in the discussion and analysis of the data. E. W. conceived and coordinated this project. The design of the experiments, analysis of the results and manuscript writing were done by X. X., Z. L., and E. W. All the authors discussed the results and contributed to the writing of the manuscript.

Conflicts of interest

There are no conflicts to declare.

Acknowledgements

We thank the EU projects OSNIRO (FP7-PEOPLE-2013-ITN, Grant agreement no.: 607585) and SUNFLOWER (FP7-ICT-2011-7, Grant number: 287594), the Swedish Research Council, the Swedish Research Council Formas, the Swedish Energy Agency and Chalmers Area of Advance Energy and the COST Action StableNextSol. MP1307 for financial support. R. A. J. J acknowledges funding from the European Research Council under the European Union's Seventh Framework Programme (FP/2007-2013)/ERC Grant Agreement no. 339031 and the Ministry of Education, Culture, and Science (NWO Gravity program 024.001.035). W. Z. and A. Y. acknowledge the Knut and Alice Wallenberg and Crafoord foundations. W. M. and Z. G. acknowledge financial support from the International Science Programme (ISP), Uppsala University, Sweden. X. M and W. M. acknowledge the support from the Ministry of Science and Technology (no. 2016YFA0200700) and NSFC (21504066, 21534003). We thank Dario Di Carlo Rasi for the IQE simulation. We thank Dr Harm van Eersel for using the python script to calculate the optical parameters in the IQE simulation. The research leading to these results received funding from the People Programme (Marie Curie Actions) of the European Union's Seventh Framework Programme (FP7/2007-2013) under REA grant agreement no. 608743. This publication reflects only the view of the authors and the European Union is not liable for any use that may be made of the information contained herein. X-ray data was acquired at beamlines 7.3.3 at the Advanced Light Source, which is supported by the Director, Office of Science, Office of Basic Energy Sciences, of the U.S. Department of Energy under Contract No. DE-AC02-05CH11231. The authors thank Chenhui Zhu at beamline 7.3.3 for assistance with data acquisition.

Notes and references

1 S. B. Darling and F. You, *RSC Adv.*, 2013, **3**, 17633–17648.
2 N. Espinosa, M. Hosel, D. Angmo and F. C. Krebs, *Energy Environ. Sci.*, 2012, **5**, 5117–5132.
3 A. J. Heeger, *Adv. Mater.*, 2014, **26**, 10–28.
4 J. Zhao, Y. Li, G. Yang, K. Jiang, H. Lin, H. Ade, W. Ma and H. Yan, *Nat. Energy*, 2016, **1**, 15027.
5 Y.-Y. Lai, Y.-J. Cheng and C.-S. Hsu, *Energy Environ. Sci.*, 2014, **7**, 1866–1883.
6 C. Cui, Y. Li and Y. Li, *Adv. Energy Mater.*, 2016, **6**, 1601251.
7 A. Anctil, C. W. Babbitt, R. P. Raffaelle and B. J. Landi, *Environ. Sci. Technol.*, 2011, **45**, 2353–2359.
8 M. Jørgensen, K. Norrman, S. A. Gevorgyan, T. Tromholt, B. Andreasen and F. C. Krebs, *Adv. Mater.*, 2012, **24**, 580–612.
9 S. M. McAfee, J. M. Topple, I. G. Hill and G. C. Welch, *J. Mater. Chem. A*, 2015, **3**, 16393–16408.
10 C. B. Nielsen, S. Holliday, H.-Y. Chen, S. J. Cryer and I. McCulloch, *Acc. Chem. Res.*, 2015, **48**, 2803–2812.
11 G. Sauvé and R. Fernando, *J. Phys. Chem. Lett.*, 2015, **6**, 3770–3780.
12 A. Facchetti, *Mater. Today*, 2013, **16**, 123–132.
13 H. Kang, W. Lee, J. Oh, T. Kim, C. Lee and B. J. Kim, *Acc. Chem. Res.*, 2016, **49**, 2424–2434.
14 S. E. Root, S. Savagatrup, A. D. Printz, D. Rodriquez and D. J. Lipomi, *Chem. Rev.*, 2017, **117**, 6467–6499.
15 T. Kim, J.-H. Kim, T. E. Kang, C. Lee, H. Kang, M. Shin, C. Wang, B. Ma, U. Jeong, T.-S. Kim and B. J. Kim, *Nat. Commun.*, 2015, **6**, 8547.
16 S. Liu, Z. Kan, S. Thomas, F. Cruciani, J.-L. Brédas and P. M. Beaujuge, *Angew. Chem., Int. Ed.*, 2016, **55**, 12996–13000.
17 Y. Guo, Y. Li, O. Awartani, J. Zhao, H. Han, H. Ade, D. Zhao and H. Yan, *Adv. Mater.*, 2016, **28**, 8483–8489.
18 Z. Li, X. Xu, W. Zhang, Z. Genene, W. Mammo, A. Yartsev, M. R. Andersson, R. A. J. Janssen and E. Wang, *J. Mater. Chem. A*, 2017, **5**, 11693–11700.
19 L. Gao, Z.-G. Zhang, L. Xue, J. Min, J. Zhang, Z. Wei and Y. Li, *Adv. Mater.*, 2016, **28**, 1884–1890.

20 Z. Li, X. Xu, W. Zhang, X. Meng, W. Ma, A. Yartsev, O. Inganäs, M. R. Andersson, R. A. J. Janssen and E. Wang, *J. Am. Chem. Soc.*, 2016, **138**, 10935–10944.

21 Y.-J. Hwang, B. A. E. Courtright, A. S. Ferreira, S. H. Tolbert and S. A. Jenekhe, *Adv. Mater.*, 2015, **27**, 4578–4584.

22 B. Fan, L. Ying, Z. Wang, B. He, X. Jiang, F. Huang and Y. Cao, *Energy Environ. Sci.*, 2017, **10**, 1243–1251.

23 H. Benten, D. Mori, H. Ohkita and S. Ito, *J. Mater. Chem. A*, 2016, **4**, 5340–5365.

24 T. Ameri, P. Khoram, J. Min and C. J. Brabec, *Adv. Mater.*, 2013, **25**, 4245–4266.

25 L. Yang, L. Yan and W. You, *J. Phys. Chem. Lett.*, 2013, **4**, 1802–1810.

26 L. Lu, M. A. Kelly, W. You and L. Yu, *Nat. Photonics*, 2015, **9**, 491–500.

27 Q. An, F. Zhang, J. Zhang, W. Tang, Z. Deng and B. Hu, *Energy Environ. Sci.*, 2016, **9**, 281–322.

28 B. M. Savoie, S. Dunaisky, T. J. Marks and M. A. Ratner, *Adv. Energy Mater.*, 2015, **5**, 1400891.

29 Y. Yang, W. Chen, L. Dou, W.-H. Chang, H.-S. Duan, B. Bob, G. Li and Y. Yang, *Nat. Photonics*, 2015, **9**, 190–198.

30 L. Lu, W. Chen, T. Xu and L. Yu, *Nat. Commun.*, 2015, **6**, 7327.

31 Z. Peng, Y. Xia, F. Gao, K. Xiong, Z. Hu, D. I. James, J. Chen, E. Wang and L. Hou, *J. Mater. Chem. A*, 2015, **3**, 18365–18371.

32 S. Liu, P. You, J. Li, J. Li, C.-S. Lee, B. S. Ong, C. Surya and F. Yan, *Energy Environ. Sci.*, 2015, **8**, 1463–1470.

33 H. Xu, H. Ohkita, Y. Tamai, H. Benten and S. Ito, *Adv. Mater.*, 2015, **27**, 5868–5874.

34 Y. Zhang, D. Deng, K. Lu, J. Zhang, B. Xia, Y. Zhao, J. Fang and Z. Wei, *Adv. Mater.*, 2015, **27**, 1071–1076.

35 S. Wang, Y. Qu, S. Li, F. Ye, Z. Chen and X. Yang, *Adv. Funct. Mater.*, 2015, **25**, 748–757.

36 W. Keawsongsaeng, J. Gasiorowski, P. Denk, K. Oppelt, D. H. Apaydin, R. Rojanathanes, K. Hingerl, M. Scharber, N. S. Sariciftci and P. Thamyongkit, *Adv. Energy Mater.*, 2016, **6**, 1600957.

37 T. H. Lee, M. A. Uddin, C. Zhong, S.-J. Ko, B. Walker, T. Kim, Y. J. Yoon, S. Y. Park, A. J. Heeger, H. Y. Woo and J. Y. Kim, *Adv. Energy Mater.*, 2016, **6**, 1600637.

38 J. Zhang, Y. Zhang, J. Fang, K. Lu, Z. Wang, W. Ma and Z. Wei, *J. Am. Chem. Soc.*, 2015, **137**, 8176–8183.

39 P. Cheng, C. Yan, Y. Wu, J. Wang, M. Qin, Q. An, J. Cao, L. Huo, F. Zhang, L. Ding, Y. Sun, W. Ma and X. Zhan, *Adv. Mater.*, 2016, **28**, 8021–8028.

40 L. Nian, K. Gao, F. Liu, Y. Kan, X. Jiang, L. Liu, Z. Xie, X. Peng, T. P. Russell and Y. Ma, *Adv. Mater.*, 2016, **28**, 8184–8190.

41 T. Liu, L. Huo, X. Sun, B. Fan, Y. Cai, T. Kim, J. Y. Kim, H. Choi and Y. Sun, *Adv. Energy Mater.*, 2016, **6**, 1502109.

42 H. Lu, J. Zhang, J. Chen, Q. Liu, X. Gong, S. Feng, X. Xu, W. Ma and Z. Bo, *Adv. Mater.*, 2016, **28**, 9559–9566.

43 T. Liu, Y. Guo, Y. Yi, L. Huo, X. Xue, X. Sun, H. Fu, W. Xiong, D. Meng, Z. Wang, F. Liu, T. P. Russell and Y. Sun, *Adv. Mater.*, 2016, **28**, 10008–10015.

44 B. Fan, W. Zhong, X.-F. Jiang, Q. Yin, L. Ying, F. Huang and Y. Cao, *Adv. Energy Mater.*, 2016, **6**, 1602127.

45 W. Zhao, S. Li, S. Zhang, X. Liu and J. Hou, *Adv. Mater.*, 2017, **29**, 1604059.

46 F. Zhao, Y. Li, Z. Wang, Y. Yang, Z. Wang, G. He, J. Zhang, L. Jiang, T. Wang, Z. Wei, W. Ma, B. Li, A. Xia, Y. Li and C. Wang, *Adv. Energy Mater.*, 2017, **7**, 1602552.

47 L. Zhong, L. Gao, H. Bin, Q. Hu, Z.-G. Zhang, F. Liu, T. P. Russell, Z. Zhang and Y. Li, *Adv. Energy Mater.*, 2017, **7**, 1602215.

48 N. Gasparini, L. Lucera, M. Salvador, M. Prosa, G. D. Spyropoulos, P. Kubis, H.-J. Egelhaaf, C. J. Brabec and T. Ameri, *Energy Environ. Sci.*, 2017, **10**, 885–892.

49 D. Baran, R. S. Ashraf, D. A. Hanifi, M. Abdelsamie, N. Gasparini, J. A. Rohr, S. Holliday, A. Wadsworth, S. Lockett, M. Neophytou, C. J. M. Emmott, J. Nelson, C. J. Brabec, A. Amassian, A. Salleo, T. Kirchartz, J. R. Durrant and I. McCulloch, *Nat. Mater.*, 2017, **16**, 363–369.

50 W. Zhao, S. Li, H. Yao, S. Zhang, Y. Zhang, B. Yang and J. Hou, *J. Am. Chem. Soc.*, 2017, **139**, 7148–7151.

51 J. Roncali, P. Leriche and P. Blanchard, *Adv. Mater.*, 2014, **26**, 3821–3838.

52 M. Helgesen, J. E. Carlé, G. A. dos Reis Benatto, R. R. Søndergaard, M. Jørgensen, E. Bundgaard and F. C. Krebs, *Adv. Energy Mater.*, 2015, **5**, 1401996.

53 C. R. McNeill, *Energy Environ. Sci.*, 2012, **5**, 5653–5667.

54 Y.-J. Hwang, B. A. E. Courtright and S. A. Jenekhe, *MRS Commun.*, 2015, **5**, 229–234.

55 R. Zhang, H. Yang, K. Zhou, J. Zhang, J. Liu, X. Yu, R. Xing and Y. Han, *J. Polym. Sci., Part B: Polym. Phys.*, 2016, **54**, 1811–1819.

56 H. Benten, T. Nishida, D. Mori, H. Xu, H. Ohkita and S. Ito, *Energy Environ. Sci.*, 2016, **9**, 135–140.

57 W. Su, Q. Fan, X. Guo, B. Guo, W. Li, Y. Zhang, M. Zhang and Y. Li, *J. Mater. Chem. A*, 2016, **4**, 14752–14760.

58 Z. Genene, J. Wang, X. Meng, W. Ma, X. Xu, R. Yang, W. Mammo and E. Wang, *Adv. Electron. Mater.*, 2016, **2**, 1600084.

59 C. M. Cardona, W. Li, A. E. Kaifer, D. Stockdale and G. C. Bazan, *Adv. Mater.*, 2011, **23**, 2367–2371.

60 G. Ren, C. W. Schlenker, E. Ahmed, S. Subramaniyan, S. Olthof, A. Kahn, D. S. Ginger and S. A. Jenekhe, *Adv. Funct. Mater.*, 2013, **23**, 1238–1249.

61 Z. Li, W. Zhang, X. Xu, Z. Genene, D. D. Carlo Rasi, W. Mammo, A. Yartsev, M. R. Andersson, R. A. J. Janssen and E. Wang, *Adv. Energy Mater.*, 2017, **7**, 1602722.

62 V. Coropceanu, J. Cornil, D. A. da Silva Filho, Y. Olivier, R. Silbey and J.-L. Brédas, *Chem. Rev.*, 2007, **107**, 926–952.

63 P. P. Khlyabich, A. E. Rudenko, R. A. Street and B. C. Thompson, *ACS Appl. Mater. Interfaces*, 2014, **6**, 9913–9919.

64 L. Gao, Z.-G. Zhang, H. Bin, L. Xue, Y. Yang, C. Wang, F. Liu, T. P. Russell and Y. Li, *Adv. Mater.*, 2016, **28**, 8288–8295.

65 L. J. A. Koster, M. Kemerink, M. M. Wienk, K. Maturová and R. A. J. Janssen, *Adv. Mater.*, 2011, **23**, 1670–1674.

66 S. R. Cowan, A. Roy and A. J. Heeger, *Phys. Rev. B: Condens. Matter Mater. Phys.*, 2010, **82**, 245207.